Articles

Mechanism of Photoinduced Decomposition of Ketoprofen

Klefah A. K. Musa, Jon M. Matxain, and Leif A. Eriksson*

Department of Natural Sciences and Örebro Life Science Center, Örebro University, 701 82 Örebro, Sweden

Received June 9, 2006

UV-induced decarboxylation of the NSAID ketoprofen, followed by activation of molecular oxygen or formation of a decarboxylated peroxide adduct, is explored using computational quantum chemistry. The excited energy surfaces reveal that the neutral species will not decarboxylate, whereas the deprotonated acid decarboxylates spontaneously in the triplet state, and with an associated 3−5 kcal/mol barrier from several low-lying excited singlet states. The observed long lifetimes of the decarboxylated anion is explained in terms of the high stability of the triplet benzoyl ethyl species with protonated carbonylic oxygen, from which there is no obvious decay channel. Mechanisms for the generation of singlet oxygen and superoxide are discussed in detail. Addition of molecular oxygen to give the corresponding peroxyl radical capable of initiating propagating lipid peroxidation reactions is also explored. The computed data explains all features of the observed experimental observations made to date on the photodegradation of ketoprofen.

Introduction

Nonsteroidal antiinflammatory drugs (NSAIDs)[a] are widely used pharmaceuticals, many of which are associated with an undisputable success in the treatment of a wide range of conditions. Despite their success, many of these compounds are also associated with adverse cutaneous side effects caused by photoinduced degradation of the compounds and/or generation of reactive oxygen species. One of the more commonly employed NSAIDs is the arylpropionic acid ketoprofen [2-(3-benzoylphenyl)propionic acid; KP], for which the *S*(+)-enantiomer has been shown to act as analgesic, antipyretic, and antiinflammatory agent, used in the treatment of rheumatoid arthritis, osteoarthritis, and ankylosis spondylitis,[1−3] as well as for nonrheumatoid diseases or postoperative pain.[4,5] KP has a very short half-life in blood plasma, between 2 and 3 h,[6] which together with the low single dosage administration required makes it a very suitable candidate for controlled release dosage.[7]

Among the side effects of the compound, severe skin reactions, hypersensitivity, myasthenia gravis, and photosensitivity have been reported.[8] It is furthermore known to reduce the metabolic activities in aged male rats.[9] Although the direct mutagenicity of the compound has been found to be very low,[10] KP-promoted formation of cyclobutane pyrimidine dimers, strand breaks, and other damage in DNA have been reported at concentrations above 10 μM.[11−14] Enhanced tumor radiosensitization caused by NSAID-induced generation of reactive oxygen species as a means for enhanced tumor treatment has therefore recently been proposed.[15]

Several detailed experimental studies of the photodegradation pathways of KP are available. The key reaction in the photodegradation is the very efficient photodecarboxylation (quantum yield $\Phi = 0.75$) of the deprotonated acid.[16] Given the pK_a of 4.7 for this weak acid, the deprotonated species is the dominant form under normal physiological conditions. The decomposition in turn generates radicals and photoproducts that enhance lipid peroxidation reactions, resulting in lytic activity on cell membranes.[17−19] KP (or its photodegradation products) has been shown to have a high singlet oxygen quantum yield ($\Phi = 0.4$) in nonpolar solvents,[20,21] whereas in buffered aqueous solution, superoxide is the dominant ROS generated.[17,21,22] Under anaerobic conditions, the final photoproduct of KP is (3-benzoylphenyl)ethane, whereas under aerobic conditions also the corresponding ethanol, ethyl hydroperoxide, and ethanone are reported to be formed.[16,17] The presence of dimeric products arising from initial photoionization leading to decarboxylation and benzylic radical intermediates have also been suggested.[21,22] Very accurate time-resolved laser flash photolysis experiments have revealed the presence, and in several cases the identities, of various intermediates in the photodegradation of KP.[21,23−27]

A proposed mechanism for the photoinduced degradation is displayed in Figure 1.[13,21,26] According to this scheme, the initial stage of KP phototoxicity involves the formation of the triplet state anionic species **B** through intersystem crossing (ISC) from the deprotonated first excited singlet state. The lifetime of the singlet state is reported to be less than 10^{-11} s, indicating a very rapid ISC to the triplet. The triplet state undergoes an initial electron shift from the carboxyl to the carbonyl oxygen with a half-life of electron transfer of about 250 ps,[21] followed by decarboxylation to the ketyl biradical **C** in less than 10 ns.[26] Decarboxylation reactions are well-known to occur for carboxylic acid triplet states.[28] An alternative pathway involving rapid decarboxylation from the excited singlet (rendering $^1\mathbf{C}^-$) followed by ISC to $^3\mathbf{C}^-$ has also been proposed.[25] Laser flash photolysis of KP in basic THF revealed a gradually decreasing absorption at 550 nm concomitant with increasing absorption at 650 nm.[27] This has been attributed to the gradual decarboxylation and formation of $^3\mathbf{C}^-$ within the sample. Protonation of compound **C** at the anionic oxygen (giving the neutral triplet/

* Corresponding author. E-mail: leif.eriksson@nat.oru.se, phone: +46 - 19 303 652; fax: +46 - 19 303 566.

[a] Abbreviations: NSAID, nonsteroidal antiinflammatory drug; KP, ketoprofen; ROS, reactive oxygen species; ISC, intersystem crossing; DFT, density functional theory; CNDO/S, complete neglect of differential overlap−singles excitations; ZPE, zero-point vibrational energy; IEFPCM, integral equation formalism of the polarized continuum model; TD-DFT, time-dependent density functional theory; LDA, local density approximation.

10.1021/jm060697k CCC: $37.00
Published on Web 03/21/2007

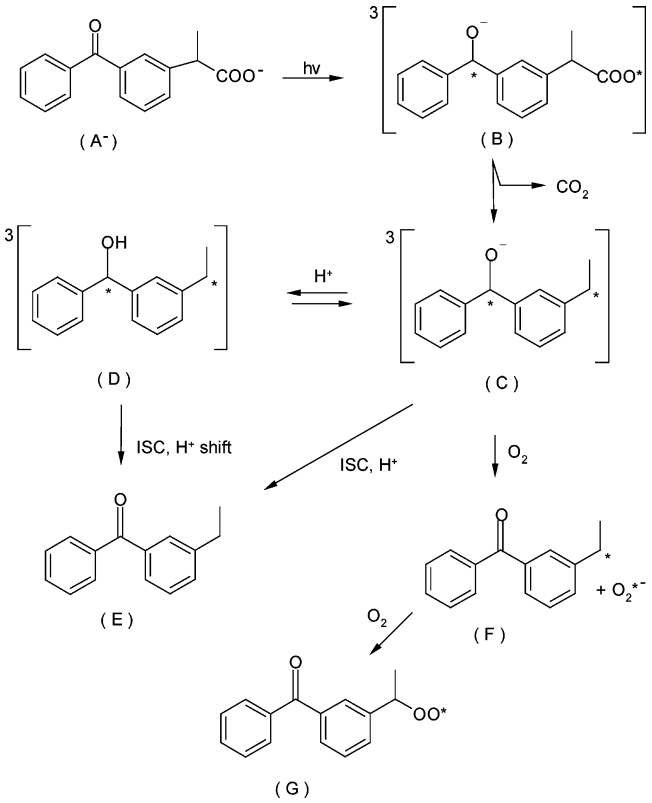

Figure 1. Proposed mechanism for UV-induced photodegradation of ketoprofen.[13,21,26] The initial steps involving excitation of $\mathbf{A}^-$ to the first excited singlet state and intersystem crossing to the triplet state (**B**), as well as alternative photoionization or singlet-mediated decarboxylation pathways, are for brevity not shown.

biradical **D**) occurs in 250−500 ns at pH < 7.6,[26] whereas **D** has a relatively long half-life, 4−10 μs, enabling a number of reactions to occur. **D** can undergo solvent-assisted proton shift and radiationless decay to the singlet ground state benzoylphenyl ethane product (**E**), or $^3\mathbf{C}^-$ can become protonated at the ethyl α-carbon directly (a process observed to dominate at pH > 7.6[26]), followed by radiationless decay to the singlet state **E**. Alternatively, the triplet anion **C** can transfer its excess electron to molecular oxygen, thereby generating superoxide anions and a benzoylphenyl ethyl radical (**F**). This may, in turn, react with a second molecule of oxygen to form the corresponding peroxyl radical **G** that is an initiator of propagating lipid peroxidation in cell membranes. Alternatively, **F** can dimerize to give 2,3-bis(3-benzoylphenyl)butane.[22] The route that is undertaken will depend on oxygen supply and on local environmental effects. It should furthermore be emphasized that direct decarboxylation from the first excited singlet state of the deprotonated acid has also been proposed; which of the two excited states that dominates the decarboxylation reaction appears to depend largely on solvent polarity.[25,29]

In the current work, the mechanistic proposal of Figure 1, including several alternative pathways such as the reactivity of the first excited singlet state of deprotonated KP and photoionization of the excited triplet followed by decarboxylation, has been explored using hybrid density functional theory (DFT) methods and a time-dependent formalism for evaluation of vertical excitation energies and UV-absorption spectra. We report optimized structures, distribution of charge and spin in the different species, and the energetics required for their formation. Of particular interest is the UV-induced decarboxylation reaction and the phototoxic reactions with molecular oxygen.

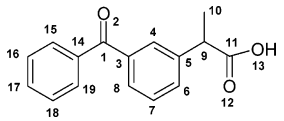

Figure 2. Atomic numbering scheme used for KP and its derivatives.

Previous computational studies of KP involve a semiempirical outline of the nature of the lowest lying excited states,[21] indicating that the lowest singlet state is of delocalized π,π^* nature, occurring at 360 nm (2.44 eV), whereas the lowest lying triplets were found at 3.08 and 3.15 eV, with very similar electronic distribution as the S_0 ground state. The lowest lying triplet is of π,π^* character according to the semiempirical calculations, whereas higher level methods predict this to have mainly n,π^* character. Lhiaubet et al.[24] performed local-density approximation (LDA) calculations within the density functional theory (DFT) framework, of the orbitals and UV excitations of the protonated form of KP (unfortunately using these results to rationalize the behavior of the deprotonated species). The orbitals obtained for KP were highly similar to those given herein for the protonated form and will be discussed later. The excited states obtained for protonated KP were found at 418 nm for n,π^* S_1 and 307 nm for the π,π^* state. Also the T_1 state was found at considerably longer wave lengths (487 nm) compared with the CNDO/S data by Monti et al. (402 nm).[21] We also mention a recent density functional theory (DFT) study of the relative energies of different rotamers of protonated ground state KP in relation to Raman spectroscopy measurements,[30] albeit being of lesser relevance to the current study.

Methods

All ground state singlet and doublet radical states, as well as excited triplet states, along the reaction pathways outlined in Figure 1 were optimized at the hybrid Hartree−Fock DFT functional B3LYP level of theory,[31−33] in conjunction with the 6-31G(d,p) basis set. In addition, the adiabatic electron affinity and ionization potential of the neutral ground state parent compound **A** were computed. Frequency calculations were performed on the optimized geometries at the same level of theory to ensure the systems to be local minima (no imaginary vibrational frequencies) and to extract zero-point vibrational energies (ZPE) and thermal corrections to the Gibbs free energies at 298 K. The numbering scheme of the atoms used throughout the study is given in Figure 2.

Solvent effects were taken into consideration implicitly, through single point calculations on the optimized geometries at the same level of theory, including the integral equation formulation of the polarized continuum model (IEFPCM).[34−36] Water was used as solvent, through the value 78.31 for the dielectric constant in the IEFPCM calculations. In order to explore in more detail the effect of the solvent on geometric structures and on the triplet state decarboxylation reaction, optimizations of certain species were also performed within the IEFPCM environment. Formation of the peroxyl radical species (**G**) was investigated by scanning the C9−O distance between 3.6 and 1.5 Å with step size 0.1 Å and in each point reoptimizing the remaining structural parameters.

Vertical singlet and triplet excitation energies of the protonated and deprotonated forms of KP were determined using the time-dependent (TD) formalism,[37−39] at the B3LYP/6-31G(d,p) level of theory. A scanning approach similar to that mentioned above was employed to investigate the decarboxylation processes of neutral and deprotonated KP, **A** and $\mathbf{A}^-$. In these cases, the ground state structures were optimized in each step while scanning the C9−C11 distance and at each optimized point computing the lowest excited singlet states. In certain cases (indicated in the text), calculations were also performed using the larger 6-31+G(d,p) basis set. All calculations were performed using the Gaussian03 program package.[40] The current methodology employed is well-known to render reaction energies accurate to within ±2 kcal/mol (~0.1 eV),

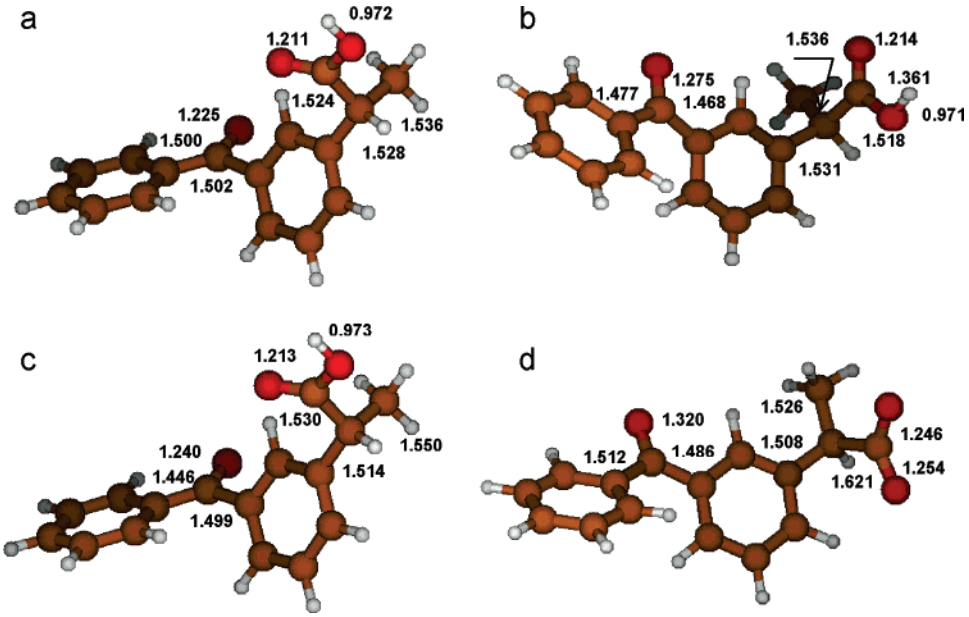

Figure 3. B3LYP/6-31G(d,p) optimized structures of (a) neutral ground state KP (**A**), (b) KP radical anion $\mathbf{A}^{\bullet-}$, (c) KP radical cation $\mathbf{A}^{\bullet+}$, (d) deprotonated KP, $\mathbf{A}^{-}$.

whereas for excitation energies the calculations tend to overestimate these by 3−5 kcal/mol (∼0.2 eV). Hence, this means that the computed absorption peaks will be blue-shifted relative to experiment, by approximately 10 nm at $\lambda = 250$ nm and by 15 nm at $\lambda = 300$ nm. The blue-shift of current TD-DFT methodology has previously been investigated in great detail, as has the effect of bulk solvation and inclusion of explicit water molecules on the absorption spectra of neutral and charged species.[41] The overall conclusion is that the influence of excplicit and implicit solvents have a very small (within a few kcal/mol) influence on the calculated spectra. Such effects are thus neglected in the current work.

Results and Discussion

A. Redox Chemistry of Ketoprofen. We begin by investigating the proton affinity and redox properties of the parent compound **A**. In Figure 3 we display the optimized structures of KP, its radical anion and radical cation ($\mathbf{A}^{\bullet-}$ and $\mathbf{A}^{\bullet+}$), and its deprotonated acid ($\mathbf{A}^{-}$). Due to steric repulsion between the two rings, these attain a dihedral angle (C8−C3−C14−C19) of 50−55° for all systems explored. This induced steric torsion efficiently reduces the delocalized conjugation over the molecule and is also reflected in the elongated C−C bonds to the central carbonyl group (1.50 Å in compound **A**), compared with the C−C bond lengths 1.39−1.41 Å in the phenyl rings. Forming the radical anion or radical cation of KP (Figure 3b and 3c, respectively) renders only marginal effects to the structures. The main changes are seen in the bonds to the carbonylic carbon C1, which can be rationalized by looking at the orbitals of the parent compound (Figure 4). The highest occupied molecular orbital (HOMO) of **A** is of *n* type localized mainly on the central carbonylic oxygen, whereas the lowest unoccupied MO (LUMO) is a π^* orbital antibonding between C1−O2 and with tails out into the phenyl rings.[24] Thus, both adding an electron to the LUMO or removal of an electron from the HOMO will primarily lead to an elongation of the C═O bond and slight reduction in the C1−C bonds.

In comparing Mulliken charges of the neutral and anionic species, however, we note that for the radical anion $\mathbf{A}^{\bullet-}$ only ∼0.24 e^- are added to the carbonyl group, whereas for the cation, 0.16 e^- are removed therefrom. Hence, in the relaxed structures, the charges delocalize into the phenyl rings, giving rise to slightly increased C−C bond lengths in these systems. The unpaired spin distributions of the radical species are given in Table 1. The unpaired electron in the radical anion is delocalized over both rings and the central carbonyl unit, with the main component on O2 (0.28 e). For the $\mathbf{A}^{\bullet+}$ cation, the unpaired spin is found on the substituted ring and on the carbonyl group, with the main component on O2 (0.49 e). Again, these pictures are consistent with the shapes of the HOMO and

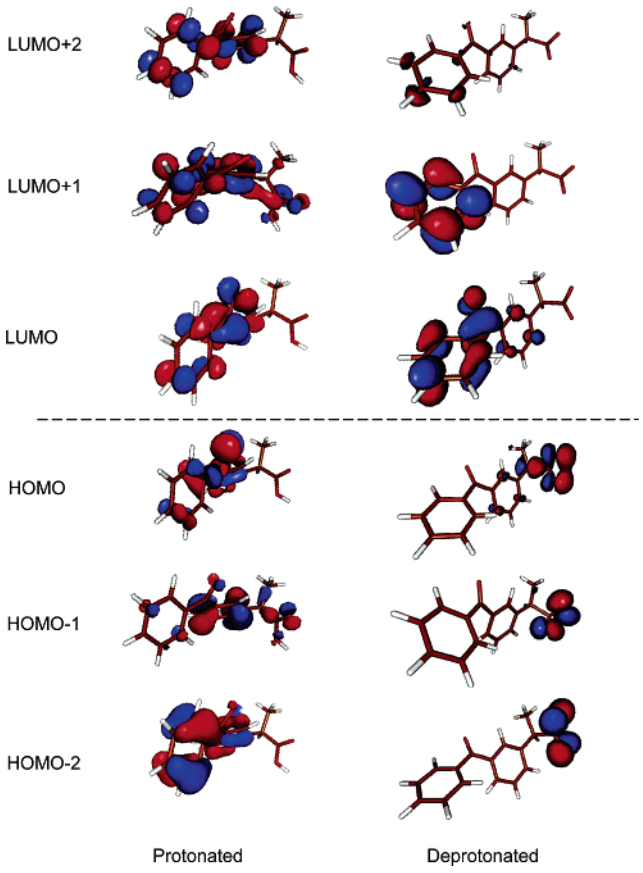

Figure 4. B3LYP/6-31+G(d,p) computed orbitals for neutral (left column) and deprotonated (right column) KP. The carboxylic group is throughout located on the right-hand side of the molecule.

Table 1. Main Unpaired Spin Components (Mulliken atomic spin densities), Obtained at the IEFPCM-B3LYP/6-31G(d,p) Level

system	C1	O2	C3	C4	C5	C6	C7	C8	C9
A$^{\bullet-}$ (doublet)	0.195	0.279	0.025	0.111	−	0.183	−	−	−
A$^{\bullet+}$ (doublet)	−0.059	0.488	0.239	0.132	−	0.183	−	−	−
B$^-$ (triplet)	0.207	0.273	−	0.374	−0.213	0.360	−0.143	0.298	0.747
C$^-$ (triplet)	0.210	0.273	−	0.375	−0.219	−0.354	−	0.297	0.762
D (triplet)	0.563	0.075	−0.226	0.431	−0.244	0.370	−0.191	0.381	0.758
F (doublet)	−	−0.018	−0.121	−1.257	−0.194	0.220	−0.123	0.249	0.772
G (doublet)	all spin on inner (0.303 e) and outer (0.692 e) peroxyl oxygens.								

Table 2. B3LYP/6-31G(d,p) Zero-Point Energy Corrected Electronic Energies in Gas Phase, and IEFPCM-B3LYP/6-31G(d,p) Gibbs Free Energies in Aqueous Solution[a]

system	$E_{(ZPE)}$	$\Delta E_{(ZPE)}$	ΔG_{aq}^{298}	$\Delta\Delta G_{aq}^{298}$	μ_{aq}
A (singlet)	−843.589559	0.0	−843.657352	0.0	5.92
A$^{\bullet-}$ (doublet)	−843.606046	−10.3	−843.746140	−55.7	8.60
A$^{\bullet+}$ (doublet)	−843.294475	+185.2	−843.417370	+150.6	4.56
A$^-$ (singlet)	−843.038319	+345.9	−843.180613	+299.2	20.33
B (triplet)	−843.491910	+61.3	−843.557354	+62.7	4.00
B$^-$ (triplet)	−842.989682	+376.4	−843.128212	+332.0	6.21
B$^\bullet$ (doublet)	−842.928359	+414.9	−842.993721	+416.4	6.44
C$^-$ (triplet)	−654.416987	0.0	−654.556844	0.0	5.99
C$^-$ (singlet)	−654.426650	−6.1	−654.547579	+5.8	11.97
D (triplet)	−654.964757	−343.7	−655.019918	−290.6	2.00
D (singlet)	−654.929834	−321.8	−654.986244	−269.5	6.89
E (triplet)	−654.940127	−328.8	−654.990239	−272.0	2.26
E (singlet)	−655.037164	−389.2	−655.088906	−333.9	4.11
F (doublet)	−654.402960	+8.8	−654.455986	+63.3	3.81
G (doublet)	−804.746072		−804.806434		3.50

[a] Absolute energies in a.u., relative energies in kcal/mol. Dipole moments μ (debye) in aqueous solution.

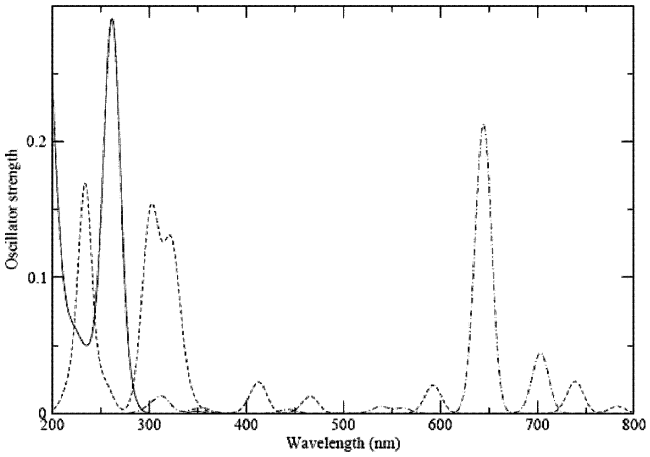

Figure 5. Computed absorption spectra of the neutral (solid) and deprotonated (dashed) forms of KP, as well as the decarboxylated anion **C**$^-$ (dot-dashed), obtained at the TD-B3LYP/6-31G(d,p) level.

LUMO orbitals of the neutral ground state system. For the carboxylic oxygens, very small components of unpaired spin are noted throughout.

For the deprotonated species, **A**$^-$, the C1−O2 (C11−O13) bonds increase (decrease) by 0.1 Å, respectively, upon removal of H13. More importantly, the C9−C11 bond increases to 1.62 Å, indicating that the anionic system may readily undergo decarboxylation. The carboxylic moiety holds approximately 0.65 e$^-$ of negative charge, whereas the charges on the central carbonyl group are essentially unaltered. The orbitals depicted in Figure 4 show that the HOMO, HOMO-1, and HOMO-2 orbitals are all centered on the carboxylic moiety of the molecule, as opposed to the situation for the protonated species. Hence, it can be expected that the photochemistry of the form present at physiological pH (**A**$^-$) will be markedly different from that of the neutral parent compound. Using the neutral compound **A** to rationalize the energetics and photochemistry of **A**$^-$ may thus lead to wrong conclusions regarding the actual mechanisms involved. The HOMO orbital is antibonding between C9 and C11, as well as between C11 and the two oxygens, which explains the structural features shown in Figure 3. Worth noting is that the unoccupied orbitals of deprotonated KP are centered on the carbonyl group and phenyl rings.

In Table 2 we list the absolute and relative ZPE-corrected energies in gas phase, the absolute and relative Gibbs free energies in aqueous solution, and the dipole moments in aqueous solution, for the different KP species investigated. We note that both in vacuo and in aqueous phase, the anionic species **A**$^{\bullet-}$ is more stable than the corresponding neutral form **A**, with a considerable stabilizing effect (45 kcal/mol) introduced by the bulk solvation. The adiabatic ionization potential in vacuo is 185 kcal/mol, whereas the aqueous solution stabilizes the cation, thereby reducing the Gibbs free energy difference to 150 kcal/mol. The free energy difference between the neutral and the deprotonated KP in aqueous solution is 299 kcal/mol.

The above-mentioned delocalization of charge in the radical anion and radical cation is well reflected in the computed dipole moments of the molecules, that only change by a few Debye relative to the neutral parent compound. This should be compared to the deprotonated acid, where the dipole moment increases by more than 14 Debye because of the highly localized negative charge on the carboxylic group.

B. Excitation of Ketoprofen and Its Deprotonated Species. The initial step in the photodegradation of KP is the excitation of **A**, in its neutral or deprotonated form, to a low-lying excited singlet state S_n, followed by intersystem crossing to a close-lying triplet state T_n. In Figure 5 we display the computed UV-spectra of of **A** and **A**$^-$. The two spectra display some interesting differences. For the neutral species, the first vertical S_1 (HOMO→LUMO) excitation occurs at 349 nm (82 kcal/mol), in the UV-regime of the spectrum, and has an oscillator strength of only 0.0007, indicative of very low probability. This is consistent with the orbitals depicted in Figure 4, showing that the excitation is of forbidden n,π* nature. The main peak occurs at 261 nm, followed by a small shoulder at 220 nm and a large number of strong absorptions at wavelengths shorter than 200 nm. Absorptions are also found at 277 and 269 nm, but with essentially negligible oscillator strengths. Similar observations were made by Lhiaubet et al. in their TD-LDA analysis[24] that the experimentally denoted S_2 state is in fact a higher lying singlet excitation. Except for the S_1 transition, all the low-lying excitations involve π,π* transitions from the highest lying occupied MO's to the LUMO.

For the deprotonated species, the lowest lying excitations are again from the highest occupied MO's to the LUMO but this time requiring energies about half of those seen for the protonated form. The excitation to the S_1 state is found already

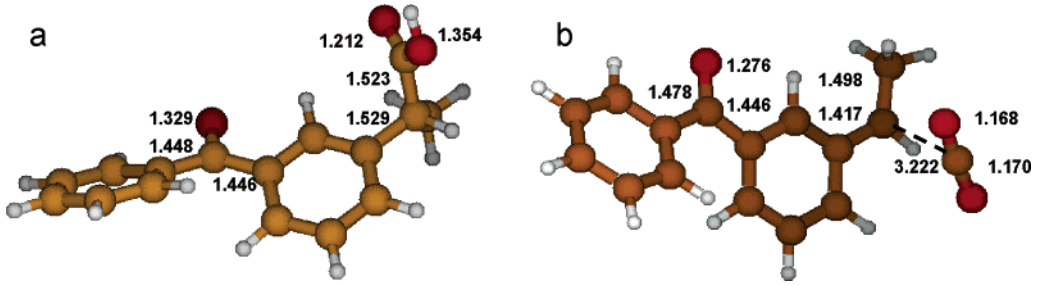

Figure 6. Optimized structures (B3LYP/6-31G(d,p) level) of (a) neutral and (b) deprotonated T_1 states of KP.

at 36.5 kcal/mol (783 nm), which is well into the red/infrared region, followed by several excitations in the visible part of the spectrum. As seen from Figure 5, all computed excitations in the $400 < \lambda < 800$ nm region are however associated with very small oscillator strengths (transition probabilities), due to the poor overlap between the highest occupied MO's (localized to the carboxylate group) and the lowest unoccupied ones (localized on the conjugated rings). Hence, the probabilities for these lowest-lying excitations to occur are too small to play any role for the photochemistry of the species. Absorptions with the largest oscillator strengths, up to 10 times stronger than those predicted in the visible region, are found at 322, 300, and 233 nm. As only the 30 lowest transitions were computed, the calculated spectrum ends at 217 nm, whereas several peaks with high oscillator strengths will be found also at higher excitation energies (shorter wavelengths). Since KP is a weak acid with pK_a 4.7, we can expect that at physiological pH in aqueous solution the system will be deprotonated. In nonpolar aprotic solvents such as isopentane, one can instead assume the system to have a higher percentage of the neutral form. As mentioned above, the photoinduced decarboxylation has been shown to occur exclusively from the deprotonated acid.[16]

Red-shifting the computed spectra for the deprotonated KP by 0.2 eV (see Methods) gives the main peaks at 242, 315, and 341 nm, which matches very well the experimental spectrum with a large peak at 250−260 nm (strong absorption attributed to the $S_0 \rightarrow S_{\prime 2\prime}$ π,π^* transition) and a shoulder in the 300−350 nm region (assigned to the forbidden $S_0 \rightarrow S_{\prime 1\prime}$ n,π^* transition) observed in pure ethanol, isopentane, and phosphate buffers at pH 7.4.[21,24] We furthermore note that the spectrum of the neutral species resembles the deprotonated form but with the small (forbidden) absorption just above 350 nm being essentially zero and a large peak at 262 nm. The currently computed data agrees far better with the experimental absorptions than those previously reported at the CNDO/S[21] or local density functional theory (TD-LDA)[24] levels of theory, the latter furthermore being performed on the neutral species only. In the semiempirical study of Monti et al.,[21] the protonation state of KP is not reported.

There are several proposals regarding the immediate fate of the excited ketoprofen. It may decarboxylate already from the short-lived excited singlet state[25,29] or undergo fast intersystem crossing to a near-by triplet state. From the triplet, fast decarboxylation gives the triplet anion **C** that in turn may protonate and quench, or react with molecular oxygen.[13,21] Decarboxylation of the triplet (or singlet) anion has been clearly shown to be the main pathway. Photoionization followed by decarboxylation and dimerization corresponds to a biphotonic pathway occurring upon excitation at 266 nm.[21]

The optimized lowest-lying triplet of the deprotonated form ($\mathbf{B}^-$) lies 32.8 kcal/mol above the optimized singlet ground state ($\mathbf{A}^-$); for the protonated species, the corresponding free energy difference is 62.7 kcal/mol. The values are very little affected by the inclusion of bulk solvation. The vertical T_1 energies obtained from the TD-DFT calculations of the neutral and deprotonated species are 67.6 and 40.8 kcal/mol, respectively, indicating the structural relaxation stabilizes the systems by 5−8 kcal/mol.

For the deprotonated system, the structural relaxation involves spontaneous decarboxylation, as seen from the optimized geometry given in Figure 6. This is consistent with the very short triplet lifetime reported: 250 ps for internal charge rearrangement from the carboxyl group to the carbonyl oxygen O2 after intersystem crossing from the excited singlet, and 10 ns for decarboxylation.[13,21,26] The optimized deprotonated triplet has the main unpaired spin component (0.75 e) on carbon C9 formerly attached to the leaving carbon dioxide, and the remainder is spread in an alternant fashion throughout the molecule; the carbonyl oxygen O2 hosts only 0.22 e of unpaired spin but has a negative charge of -0.62 e$^-$, again consistent with the proposed scheme, albeit with the modification that carbon C1 is not the main center for the second unpaired electron. In fact, this harbors approximately 0.33 e of unpaired spin, which is very similar to every second carbon in the substituted benzene ring (cf. Table 2). The computations are, however, unable to verify the existence of a very short-lived intermediate with the negative charge localized to carbon C9, as proposed in ref 26.

For the protonated species, the main geometrical changes when optimizing the triplet state occur around the carbonyl group (elongated C1═O2 bond and shortened C1−C bonds). These geometrical changes are readily accounted for when considering the orbitals involved; see Figure 4. In the neutral T_1 state, one of the unpaired electrons is localized entirely to the carbonyl oxygen, and the other is distributed on alternating carbons with the main component on the carbonyl carbon C1 (0.46 e) and 0.14−0.19 e on the remaining alternant ring carbons. Energetically, the initial $S_0 \rightarrow S_1$ excitation energy of the neutral system requires approximately 82 kcal/mol; following ISC to the T_1, this will relax to a free energy located 63 kcal/mol above S_0. For the neutral triplet to deprotonate requires 269.3 kcal/mol of energy, i.e., considerably less than for the singlet ground state deprotonation (299 kcal/mol), and is comparable to the free energy of a solvated proton (268.7 kcal/mol[42]). Exciting the neutral species, we can assume that provided the ISC to the triplet is sufficiently rapid to occur before quenching of the S_1 state, the compound will more or less spontaneously deprotonate and then, in turn, spontaneously decarboxylate.

In order to investigate if the excited singlet states may also spontaneously decarboxylate, the C9−C11 bond was scanned outward from the optimized value of the neutral and the deprotonated forms of KP (1.524 and 1.621 Å, respectively), in steps of 0.1 Å. In each new point, the structures were reoptimized, and the vertical excitations were calculated. The

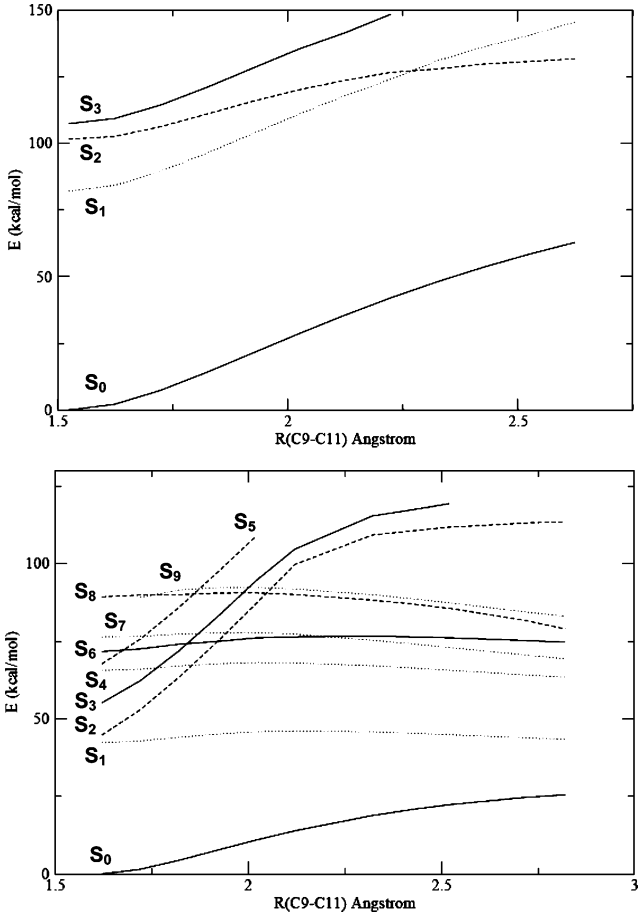

Figure 7. Energy curves for decarboxylation of the neutral (top) and deprotonated (bottom) KP. The ground state and some of the lowest excited singlet states are shown for each system.

resulting energy curves, obtained at the TD-B3LYP/6-31+G-(d,p) level, are displayed in Figure 7 which includes a set of the lowest singlet excitations for each system. As expected, the neutral species shows no sign of decarboxylation, as the ground state and three lowest excited singlet state energies are strictly endothermic throughout the scan of the C−C bond.

For the deprotonated species, the situation is markedly different. Of the lower-lying (undetectable) singlets, the S_2, S_3, and S_5 states appear to be strictly endergonic. The S_6-S_9 excitations with main oscillator strengths (at 322, 300, and 233 nm; cf. Figure 5) all show exergonic decarboxylation reactions proceeding by way of a small energy barrier, of the order of 2−3 kcal/mol, at C−C distances between 1.8−2.1 Å. Hence, several of the excited singlet states of the deprotonated system can be expected to result in a decarboxylated species $^1\mathbf{C}^-$, if the system is capable of residing in the state for a sufficiently long time. Noteworthy in this context is that the experimentally estimated S → T ISC of deprotonated KP^- has been determined to be less than 10^{-11} s.[13] Associated with the singlet excited states are also various triplet states in general lying ca. 5 kcal/mol below the corresponding singlet excited states. The energy gap from S_0 is 40.8, 45.3, 55.6, 65.5, 67.9, 69.4, 70.5, 74.7, and 76.2 kcal/mol for the T_1-T_9 sequence. The consistently small S−T gap is quite unusual and opens up for several possibilites to rapid ISC. Of particular interest is the T_6 state, which is strongly dominated by excitation from the HOMO-1 to the LUMO+1 orbital (cf. Figure 4), and lies 69.4 kcal/mol above the anionic ground state. This also agrees with the experimental value for the "T_1" state determined in isopentane, at 423.5 nm (67.5 kcal/mol; 69.3 kcal/mol in ethanol), after excitation at $\lambda = 313$ nm.[24] The higher-lying triplets include components from more orbitals but are all associated with the orbital manifold displayed in Figure 4. On the basis of the results obtained for the decarboxylation process, it is apparent that the disparate observations made experimentally in most cases can be attributed to local effects of the surrounding and different experimental lifetimes.

Provided that the excited states of the neutral or deprotonated species are sufficiently long-lived to interact with oxygen molecules directly, we furthermore note that they will in principle be capable of generating either superoxide or singlet oxygen, the latter concomitant with relaxation to the S_0 ground state. On the other hand, given the short lifetimes and spontaneous deprotonation/decarboxylation reactions of the excited species, the generation of ROS appear to be more likely to occur from species **C**/**D** than from the initial carboxylated species.

C. The Decarboxylated Radical C. Once decarboxylation has occurred, the resulting carbanion $\mathbf{C}^-$ may undergo several reactions, as indicated in Figure 1. Assuming decarboxylation to occur from the excited singlet state, the stability of $^1\mathbf{C}^-$ is of interest. However, as the singlet is calculated to be approximately 6 kcal/mol less stable than the triplet form, we can assume this to undergo relatively rapid ISC to $^3\mathbf{C}^-$. An activation energy of 3.2 kcal/mol has been reported for the decay of the short-lived transient $^3\mathbf{C}^-$, absorbing with a maximum at around 580 nm and disappearing on the 100 ns time scale.[25] In the work by Laferriére et al., an initial peak at around 550 nm of the transient intermediate formed immediately after laser flash photolysis and was seen to decay and a peak at around 660 nm increase, in the 1−200 μs time scale.[27] This change in spectrum has been attributed to the completed decarboxylation of the initial excited system. In Figure 5 we include the computed absorption spectrum (15 lowest singlet excitations) of species $^3\mathbf{C}^-$. As seen from the graph, the spectrum of the fully decarboxylated species displays one large absorption at 644 nm, which agrees well with the findings of Laferriére et al.

Protonation of the radical anion to generate the singlet form of the benzoyl phenyl ethane **E** will involve protonation and intersystem crossing and possibly also a proton or hydrogen atom shift. The pK_a value (7.6)[21] of the triplet anion $^3\mathbf{C}^-$ indicates that the system at physiological pH is close to equilibrium between $\mathbf{C}^-$ and the triplet form of either **D** or **E**, differing in the site of protonation. The negative charge of the anion is accumulated on the carbonyl oxygen (−0.62 e$^-$), and we may thus expect this to be the preferred site for protonation. This is also manifested in that energetically the oxygen-protonated species ^{3}**D** is 19 kcal/mol more stable than ^{3}**E.** The energy of formation of $^3\mathbf{D}$ from $^3\mathbf{C}^-$ is 290.6 kcal/mol, and that of $^3\mathbf{E}$ is 272.0 kcal/mol. Comparing this to the value estimated for the solvated proton, 268.7 kcal/mol,[42] we conclude that either of the two will be formed spontaneously in the presence of protons in solution, and that $^3\mathbf{D}$ is thermodynamically more stable. The triplet form of compound **D** has been shown to have a long lifetime (4 μs),[21] which is attributed to the non-Kekulé structure of the conjugated fragments. The difference in enthalpy between species $^3\mathbf{C}^-$ and $^3\mathbf{D}$ is approximately 18 kcal/mol,[25] which agrees with the calculated free energy difference between the two species (adding also the energy of a solvated proton), amounting to 21.9 kcal/mol.

The different pathways leading from $^3\mathbf{C}^-$ to $^1\mathbf{E}$ can be envisaged as follows,

$$^3\mathbf{C}^- \xrightarrow{+H^+} {}^3\mathbf{D} \xrightarrow{H^+\ \text{shift}} {}^3\mathbf{E} \xrightarrow{ISC} {}^1\mathbf{E} \qquad (1)$$

$$^3\mathbf{C}^- \xrightarrow{+H^+} {}^3\mathbf{D} \xrightarrow{ISC} {}^1\mathbf{D} \xrightarrow{H^+\ shift} {}^1\mathbf{E} \quad (2)$$

$$^3\mathbf{C}^- \xrightarrow{+H^+} {}^3\mathbf{E} \xrightarrow{ISC} {}^1\mathbf{E} \quad (3)$$

$$^3\mathbf{C}^- \xrightarrow{ISC} {}^1\mathbf{C}^- \xrightarrow{+H^+} {}^1\mathbf{E} \quad (4)$$

Having formed the protonated species **D**, it is unlikely that this will undergo solvent-mediated hydrogen/proton transfer to form ^{3}**E** (reaction 1), given the large energy difference between the two. If occurring, this will be a slow process, as indicated by the long lifetime of the ^{3}**D** species. The decay from triplet to ground state singlet form of **E** is exothermic by 62 kcal/mol. If we instead assume the ^{3}**D** takes the route by way of the lowest lying singlet form of **D** (reaction 2), this is also seen to be hindered energetically, as the ^{1}**D** form lies 21 kcal/mol above ^{3}**D**. Compound **D** hence has a triplet ground state, due to the meta-positions of the carbonyl and ethyl radical positions, that efficiently disallows resonance conjugation in the closed shell singlet form. The factors outlined so far thus speak in favor of ^{3}**D** being formed from ^{3}**C**$^-$ but with very few options to quench and form the ^{1}**E** product. Protonation of the ethylene radical site in ^{3}**C**$^-$ (reaction 3), followed by or concomitant with decay to the singlet, instead appears as a more viable route to ^{1}**E**. ^{3}**E** is slightly more stable than the energy of ^{3}**C**$^-$ and a solvated proton, and ^{1}**E** is another 62 kcal/mol more stable. A stepwise protonation + decay pathway ^{3}**C**$^- \rightarrow {}^3$**E** $\rightarrow {}^1$**E** thus appears to be a likely route. Again, this explains the long lifetime of the system, in that it can become 'trapped' in the ^{3}**D** form, with only slow leakage back, and alternative protonation to ^{3}**E**.

One may in principle also envision a pathway involving ISC or decay of the initial triplet radical anion to the corresponding singlet anion ^{1}**C**$^-$ (reaction 4). This would involve large charge redistribution, as is manifested in the significant increase in dipole moment, and again leads to a non-Kekule type of structure. Therefore, in aqueous solution the singlet form is 6 kcal/mol less stable than the triplet, and also for reaction 4 do we find the initial (ISC) step to be endergonic, efficiently hindering the pathway. Hence, the triplet state of **C**$^-$ will not be capable of transferring its excitation energy to molecular oxygen in order to generate reactive singlet oxygen species. This is however fully possible in reaction 3, where the triplet to singlet decay of compound **E** provides significant energy for excitation of O_2. The path leading to ^{1}**E** may hence serve as an efficient route to the formation of singlet oxygen.

Another fate of compound ^{3}**C**$^-$ is for the species to undergo electron transfer to molecular oxygen, in order to generate superoxide radical anions. That is, ^{3}**C**$^- + O_2 \rightarrow {}^2$**F** $+ {}^2O_2^-$. Due to the large stabilization of the charged species by the polar solvent, the anion ^{3}**C**$^-$ is 63.3 kcal/mol more stable than the ionized radical ^{2}**F** in aqueous solution (Table 3). This should be compared with the adiabatic electron affinity of molecular oxygen to generate superoxide in solution, estimated to 90.2 kcal/mol (3.91 eV),[41] which implies that the overall reaction will be exergonic by approximately 27 kcal/mol. Irreversible quenching of the triplet anion by oxygen-dependent electron transfer to form the benzylic radical **F** and superoxide is thus very likely to occur under aerobic conditions in polar media.

The above results explain the experimental observations (see introduction) that only the benzoylphenyl ethane **E** is formed under anaerobic conditions, whereas aerobically we also see various oxygenated species (arising from subsequent addition of oxygen to the radical site of ^{2}**F**). That polar media increases the production of superoxide over that of singlet oxygen is also explained by the current results, due to the large solvent-induced stabilization (increased electron affinity) of the superoxide radical anion.

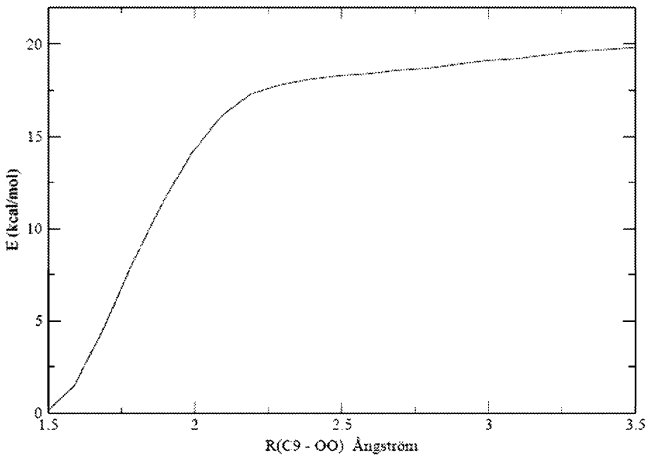

Figure 8. Reaction path for formation of peroxyl radical **G** from ^{2}**F** and molecular oxygen.

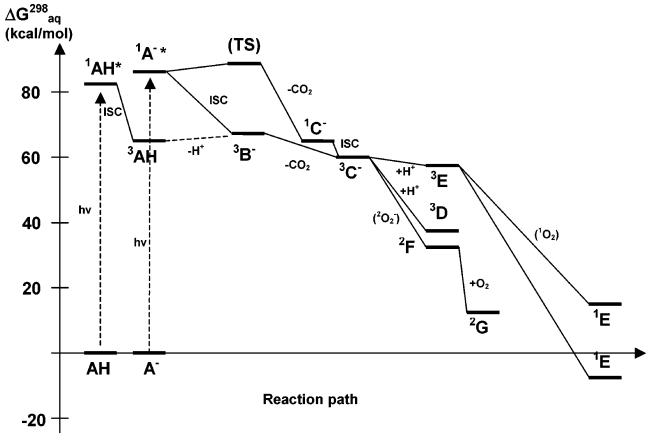

Figure 9. Approximate relative Gibbs free energy diagram for the photodegradation of ketoprofen in aqueous solution. In each separate reaction step, the energies of all involved reacting species are included (e.g., the energy of a solvated proton is included when determining the ^{3}**C**$^- \rightarrow {}^3$**E** reaction energy and so forth). The energy curve is based on excitation to the first dominant excited state within the S_6-S_9 manifold.

The addition of molecular oxygen to the benzylic radical ^{2}**F** to generate the peroxyl radical ^{2}**G** has been postulated to not only give the various oxygenated derivatives mentioned above but also to initiate lipid peroxidation reactions.[21] The peroxyl radical **G** will in this scenario abstract a hydrogen atom from a lipid molecule (L), that through addition of molecular oxygen to the new L$^\bullet$ radical site creates the propagating radical damage.

$$^2\mathrm{F}^\bullet + \mathrm{O_2} \rightarrow {}^2\mathrm{G(OO^\bullet)} \quad (5)$$

$$^2\mathbf{G(OO^\bullet)} + \mathrm{LH} \rightarrow \mathbf{G(OOH)} + \mathrm{L}^\bullet \quad (6)$$

$$\mathrm{L}^\bullet + \mathrm{O_2} \rightarrow \mathrm{LOO}^\bullet \quad (7)$$

$$\mathrm{LOO}^\bullet + \mathrm{LH} \rightarrow \mathrm{LOOH} + \mathrm{L}^\bullet \quad (8)$$

Once initiated, the chain reactions 7 and 8 will then repeat until terminated by, e.g., radical−radical addition or the action of an antioxidant such as vitamin E. In ^{2}**F** the main fraction of the unpaired spin (0.77 e) is located to carbon C9. The addition reaction with molecular oxygen in its $^3\Sigma$ ground state to form

^{2}**G** was explored by scanning the C9−O_2 distance in steps of 0.1 Å; the energy diagram for this process is displayed in Figure 8. The energy difference between the peroxyl radical product ^{2}**G** and that where the two reactants are separated by 3.5 Å, is close to 20 kcal/mol, and the addition reaction is strictly exothermic, with a clear change in slope at a C−O distance less than 2.1 Å. The generation of the peroxyl radical is hence also strictly exergonic under aerobic conditions; in the presence of molecular oxygen, reaction 5 will occur spontaneously and without any barrier.

Conclusions

We have in the current work explored the photochemistry of the NSAID ketoprofen. The absorption spectra reveal that the deprotonated species, which is the dominant form under physiological conditions, has several low-lying excitations in the 400−800 nm range, albeit with very low probability. The main excitations are calculated to occur at 322, 300 and 233 nm, in very good agreement with experimental data. Exploring the geometries of the excited triplet states, and scanning the C9−C11 distance on the excited singlet surfaces, it is concluded that the well-known photoinduced decarboxylation reaction can only occur for the deprotonated acid, whereas the neutral form shows no sign thereof. However, deprotonation from the T_1 state of the neutral species is found to be energetically viable, which may in turn be accompanied by decarboxylation of the anion thus formed.

For the anion, several of the excited singlet states are concluded lead to exothermic decarboxylation reactions, after passing over a small barrier (2−3 kcal/mol). The triplet of KP^-, on the other hand, undergoes spontaneous (barrier-free) decarboxylation. In addition, the excited singlet and triplet states of the deprotonated acid lie within a few kcal/mol in energy. These data explain the very high quantum yield observed for intersystem crossing and formation of the triplet, and the very short lifetime thereof. The different behavior of the neutral and deprotonated acid is explained in terms of the markedly different orbitals seen for the two species.

Once the decarboxylated triplet state anion (^{3}**C**$^-$) is formed, there are several pathways possible. The observed long lifetimes of the triplet state are explained in terms of protonation of the carbonylic oxygen (the main negative site in **C**) to give the triplet form of compound **D**. From ^{3}**D** there is no obvious route to ISC or hydrogen/proton shift in order to reach the ground state singlet of the benzoyl ethane product **E**. Instead, the route from ^{3}**C**$^-$ to ^{1}**E** is suggested to proceed by way of the less stable ethyl-protonated ^{3}**E**, followed by ISC and decay, and possible generation of singlet oxygen. Alternatively, in presence of molecular oxygen, electron transfer from **C** is possible, which generates a benzoyl ethyl radical (^{2}**F**) and superoxide. The benzoyl ethyl radical can add a second molecule of oxygen to the radical site in a strictly exothermic reaction, giving a peroxyl radical (**G**) that may either initiate lipid peroxidation or undergo further oxidation to the corresponding alcohol or keto forms.

The overall reactions schemes with relative Gibbs fee energies are summarized in Figure 9. In the figure, we include the different components belonging to each reaction step. Hence, for the pathway **C** → **F** we also include the reaction energy for creating one superoxide radical anion molecule, whereas in the step **F** → **G**, a molecule of O_2 is incorporated at the ^{2}**F** level (thus reflecting the reaction energies seen in Figure 8). In addition, the two ^{1}**E** levels differ in that one incorporates the energy required to donate excitation energy in order to generate singlet oxygen.

The computed energetics explain all observations made to date on the photochemistry of KP, including the different views on the origin of the decarboxylation reaction, and also rules out some proposed hypotheses such as the conversion channel from ^{3}**D** to the benzoylphenyl ethane system ^{1}**E**.

Acknowledgment. The MENA program (K.A.K.M.), the Wood Ultrastructure Research Center (WURC; J.M.M.), and the Swedish Science Research Council (L.A.E.) are gratefully acknowledged for financial support. We also acknowledge generous grants of computing time at the National Supercomputing Center (NSC) in Linköping.

References

(1) Catchart, B. J.; Vince, J. D.; Gordon, A. J.; Bell, M.; Chalmers, I. M. Studies on 2-(3-benzoylphenyl) propionic acid ('Orudis'). *Ann. Rheum. Dis.* **1973**, *32*, 62−65.
(2) Fossgreen, J.; Kirchheiner, B.; Petersen, F. O.; Tophoj, E.; Zachariae, E. Clinical evaluation of ketoprofen (19.583 R.P.) in rheumatoid arthritis-double-blind cross-over comparision with indomethacin. *Scand. J. Rheumatol.* **1976**, 93−98.
(3) Julou, L.; Guyonnet, J. C.; Ducrot, R.; Fournel, J.; Pasquet, J. Ketoprofen (19.583 R.P.) (2-(3-benzoylphenyl)-propionic acid). Main pharmacological properties: outline of toxicological and pharmacokinetic data. *Scand. J. Rheumatol.* **1976**, 33−44.
(4) Avouac, B.; Teule, M. Ketoprofen: the European experience. *J. Clin. Pharmacol.* **1988**, *28*, S2−S7.
(5) Woltex, A. *Drug facts and comparisons*; Kluwer: St. Louis, MO, 1995; pp 1272−1277.
(6) Martindale. *The extra pharmacopoeia*; The Pharmaceutical Press: London, 1996.
(7) See: Vueba, M. L.; Batista de Carvalho, L. A. E.; Veiga, F., Sousa, J. J.; Pina, M. E. Influence of cellulose ether polymers on ketoprofen release from hydrophilic matrix tablets. *Eur. J. Pharm. Biopharm.* **2004**, *58*, 51−59; and references therein.
(8) Valsecchi, R.; Falgheri, G.; Cianelli, T. Contact dermatitis from ketoprofen. *Contact Dermatitis* **1983**, *9*, 163−164.
(9) Satterwhite, J. H.; Boudinot, F. D., Pharmacokinetics of ketoprofen in rats; effect of age and dose. *Biopharm. Drug Dispos.* **1992**, *13*, 197−212.
(10) Philipose, B.; Singh, R.; Khan, K. A.; Giri, A. K. Comparative mutagenic and genotoxic effects of three propionic acid derivatives ibuprofen, ketoprofen and naproxen. *Mutat. Res.* **1997**, *393*, 123−131.
(11) Chouini-Lalanne, N.; Defais, M.; Paillous, N. Nonsteriodal anti-inflammatory drug-photosensitized formation of pyrimidine dimer in DNA. *Biochem. Pharmacol.* **1998**, *55*, 441−446.
(12) Marguery, M. C.; Chouini-Lalanne, N.; Ader, J. C.; Paillous, N. Comparison of the DNA damage photoinduced by fenofibrate and ketoprofen, two phototoxic drugs of parent structure. *Photochem. Photobiol.* **1998**, *68*, 679−684.
(13) Radschuweit, A.; Rüttinger, H.-H.; Nuhn, P.; Wohlrab, W.; Huschka, Chr. UV-induces formation of hydrogen peroxide based on the photochemistry of ketoprofen. *Photochem. Photobiol.* **2001**, *73*, 119−127.
(14) Lhiaubet, V.; Paillous, N.; Chouini-Lalanne, N. Comparison of DNA damage photoinduced by ketoprofen, fenofibric acid and benzophenone via electron and energy transfer. *Photochem. Photobiol.* **2001**, *74*, 670−678.
(15) Crockart, N.; Radermacher, K.; Jordan, B. F.; Baudelet, C., Cron, G. O.; Grégoire, V.; Beghein, N.; Bouzin, C.; Feron, O.; Gallez, B. Tumor radiosensitizationby anti-inflammatory drugs: evidence for a new mechanism involving the oxygen effect. *Cancer Res.* **2005**, *65*, 7911−7916.
(16) Boscá, F.; Miranda, M. A.; Carganico, G.; Mauleón, D. Photochemical and photobiological properties of ketoprofen associated with the benzophenone chromophore. *Photochem. Photobiol.* **1994**, *60*, 96−101.
(17) Costanzo, L. L.; De Guidi, G.; Condorelli, G.; Cambria, A.; Fama, M. Molecular mechanism of drug photosensitization − II. Photochemolysis sensitized by ketoprofen. *Photochem. Photobiol.* **1989**, *50*, 359−365.
(18) Condorelli, G., De Guidi, G.; Giuffrida, S.; Costanzo, L. Photosensitizing action of nonsteriodal antiinflammatory drugs on cell membranes and design of protective systems. *Coord. Chem. Rev.* **1993**, *125*, 115−128.

(19) Boscá, F.; Carganico, G.; Castell, J. V.; Gómez-Lechón, M. J.; Hernandez, D.; Mauleón, D.; Martínez, L. A.; Miranda, M. A. Evaluation of ketoprofen (R, S and R/S) phototoxiticy by a battery of in vitro assays. *J. Photochem. Photobiol. B: Biology* **1995**, *31*, 133−138.
(20) De la Peña, D.; Marti, C.; Nonell, S.; Martinez, L. A.; Martinez, M. A. Time resolved near infrared studies on singlet oxygen production by the photosensitizing 2-aryl-propoinic acids. *Photochem. Photobiol.* **1997**, *65*, 828−832.
(21) Monti, S.; Sortino, S.; De Guidi, G.; Marconi, G. Photochemistry of 2-(3-benzoylphenyl)propionic acid (ketoprofen), Part 1. A picosecond and nanosecond time resolved study in aqueous solution. *J. Chem. Soc. Faraday Trans.* **1997**, *93*, 2269−2275.
(22) Nakajima, A.; Tahara, M.; Yoshimura, Y.; Nakazawa, H. Determination of free radicals generated from light exposed keotprofen. *J. Photochem. Photobiol. A: Chemistry* **2005**, *174*, 89−97.
(23) Martinez, L. A.; Scaiano, J. C., Transient intermediates in the laser flash photolysis of ketoprofen in aqueous solutions: Unusual photochemistry for the benzophenone chromophore. *J. Am. Chem. Soc.* **1997**, *119*, 11066−11070.
(24) Lhiaubet, V.; Gutierrez, F.; Penaud-Berruyer, F.; Amoyal, E.; Daudey, J.-P.; Poteau, R.; Chouini-Lalanne, N.; Paillous, N. Spectroscopic and theoretical studies of the excited states of fenofibric acid and ketoprofen in relation with their photosensitizing properties. *New J. Chem.* **2000**, *24*, 403−410.
(25) Cosa, G.; Martínez, L. A.; Scaiano, J. C. Influence on solvent polarity and base concentration on the photochemistry of ketoprofen: independent singlet and triplet pathways. *Phys. Chem. Chem. Phys.* **1999**, *1*, 3533−3537.
(26) Borsarelli, C. D.; Braslavsky, S. E.; Sortino, S.; Marconi, G.; Monti, S. Photodecarboxylation of ketoprofen in aqueous solution. A time-resolved laser-induced optoacoustic study. *Photochem. Photobiol.* **2000**, *72*, 163.
(27) Laferrière, M., Sanramè, C. N.; Scaiano, J. C., A remarkably long-lived benzyl carbanion. *Org. Lett.* **2004**, *6*, 873−875.
(28) Turro, N. J., *Modern Molecular Photochemistry*; University Science Books: Sausalito, CA, 1978/1991.
(29) Cosa, G. Photodegradation and photosensitization in pharmaceutical products: Assessing drug phototoxicity. *Pure Appl. Chem.* **2004**, *76*, 263−275.
(30) Vueba, M. L.; Pina, M. E.; Veiga, F.; Sousa, J. J., Batista de Carvalho, L. A. E. Conformational study of ketoprofen by combined DFT calculations and Raman spectroscopy. *Int. J. Pharm.* **2006**, *307*, 56−65.
(31) Becke, A. Density-functional thermochemistry. III. The role of exact exchange. *J. Chem. Phys.* **1993**, *98*, 5648−5652.
(32) Lee, C.; Yang, W.; Parr, R. G. Development of the Colle-Salvetti correlation-energy formula into a functional of the electron density. *Phys. Rev. B* **1988**, *37*, 785−789.
(33) Stephens, P. J.; Devlin, F. J.; Chabalowski, C. F.; Frisch, M. J. Ab Initio calculation of vibrational absorption and circular dichroism spectra using density functional force fields. *J. Phys. Chem.* **1994**, *98*, 11623−11627.
(34) Cancès, M. T.; Mennucci, B.; Tomasi, J. A new integral equation formalism for the polarizable continuum model: Theoretical background and applications to isotropic and anisotropic dielectrics. *J. Chem. Phys.* **1997**, *107*, 3032−3041.
(35) Mennucci, B.; Tomasi, J. Continuum solvation models: A new approach to the problem of solute's charge distribution and cavity boundaries. *J. Chem. Phys.* **1997**, *106*, 5151−5158.
(36) Cossi, M.; Scalmani, G.; Rega, N.; Barone, V. New developments in the polarizable continuum model for quantum mechanical and classical calculations on molecules in solution *J. Chem. Phys.* **2002**, *117*, 43−54.
(37) Bauernschmitt, R.; Ahlrichs, R. Treatment of electronic excitations within the adiabatic approximation of time dependent density functional theory. *Chem. Phys. Lett.* **1996**, *256*, 454−464.
(38) Casida, M. E.; Jamorski, C.; Casida, K. C.; Salahub, D. R. Molecular excitation energies to high-lying bound states from time-dependent density-functional response theory: Characterization and correction of the time-dependent local density approximation ionization threshold. *J. Chem. Phys.* **1998**, *108*, 4439−4449.
(39) Stratmann, R. E.; Scuseria, G. E.; Frisch, M. J. An efficient implementation of time-dependent density-functional theory for the calculation of excitation energies of large molecules. *J. Chem. Phys.* **1998**, *109*, 8218−8224.
(40) Gaussian 03, Revision B.02, Frisch, M. J.; Trucks, G. W.; Schlegel, H. B.; Scuseria, G. E.; Robb, M. A.; Cheeseman, J. R.; Montgomery, J. A., Jr.; Vreven, T.; Kudin, K. N.; Burant, J. C.; Millam, J. M.; Iyengar, S. S.; Tomasi, J.; Barone, V.; Mennucci, B.; Cossi, M.; Scalmani, G.; Rega, N.; Petersson, G. A.; Nakatsuji, H.; Hada, M.; Ehara, M.; Toyota, K.; Fukuda, R.; Hasegawa, J.; Ishida, M.; Nakajima, T.; Honda, Y.; Kitao, O.; Nakai, H.; Klene, M.; Li, X.; Knox, J. E.; Hratchian, H. P.; Cross, J. B.; Bakken, V.; Adamo, C.; Jaramillo, J.; Gomperts, R.; Stratmann, R. E.; Yazyev, O.; Austin, A. J.; Cammi, R.; Pomelli, C.; Ochterski, J. W.; Ayala, P. Y.; Morokuma, K.; Voth, G. A.; Salvador, P.; Dannenberg, J. J.; Zakrzewski, V. G.; Dapprich, S.; Daniels, A. D.; Strain, M. C.; Farkas, O.; Malick, D. K.; Rabuck, A. D.; Raghavachari, K.; Foresman, J. B.; Ortiz, J. V.; Cui, Q.; Baboul, A. G.; Clifford, S.; Cioslowski, J.; Stefanov, B. B.; Liu, G.; Liashenko, A.; Piskorz, P.; Komaromi, I.; Martin, R. L.; Fox, D. J.; Keith, T.; Al-Laham, M. A.; Peng, C. Y.; Nanayakkara, A.; Challacombe, M.; Gill, P. M. W.; Johnson, B.; Chen, W.; Wong, M. W.; Gonzalez, C.; Pople, J. A. Gaussian, Inc., Wallingford CT, 2004.
(41) Ristilä, M.; Matxain, J. M.; Strid, Å.; Eriksson, L. A. pH-dependent electronic and spectroscopic properties of pyridoxine (vitamin B_6). *J. Phys. Chem. B* **2006**, *110*, 16774−16780.
(42) Llano, J.; Eriksson, L. A. First principles electrochemistry: Electrons and protons reacting as independent ions. *J. Chem. Phys.* **2002**, *117*, 10193−10206.

JM060697K